N O T I C E

THIS DOCUMENT HAS BEEN REPRODUCED FROM MICROFICHE. ALTHOUGH IT IS RECOGNIZED THAT CERTAIN PORTIONS ARE ILLEGIBLE, IT IS BEING RELEASED IN THE INTEREST OF MAKING AVAILABLE AS MUCH INFORMATION AS POSSIBLE

(NASA-TM-80654) SOME 1.0 mm MAPS AND RADIAL DENSITY DISTRIBUTIONS OF SOUTHERN HII/MOLECULAR CLOUD COMPLEXES (NASA) 33 p HC A03/MF A01 CSCL 03A
N80-22146
Unclas
G3/89 18131

NASA

Technical Memorandum **80654**

1.0 mm Maps and Radial Density Distributions of Southern HII/Molecular Cloud Complexes

L. H. Cheung, J. A. Frogel, D. Y. Gezari and M. G. Hauser

February 1980

National Aeronautics and Space Administration

Goddard Space Flight Center
Greenbelt, Maryland
20771

RECEIVED NASA STI FACILITY ACCESS DEPT.

1.0 mm MAPS AND RADIAL DENSITY DISTRIBUTIONS OF SOUTHERN HII/MOLECULAR CLOUD COMPLEXES

L. H. Cheung[*+], J. A. Frogel[‡], D. Y. Gezari[§+] and M. G. Hauser[§]

Submitted to Astrophysical Journal

Received _____ .

[*]Dept. of Physics, University of Maryland, and NASA Goddard Space Flight Center

[+]Visiting Astronomer at Cerro Tololo Inter-American Observatory

[‡]Cerro Tololo Inter-American Observatory,
CTIO is supported by the National Science Foundation under Contract AST 74-04128.

[§]NASA Goddard Space Flight Center

ABSTRACT

1.0 mm continuum mapping observations have been made of seven southern hemisphere HII/molecular cloud complexes with 65 arcsec resolution. The radial density distribution of the clouds with central luminosity sources was determined observationally to be $\rho(r) \propto r^{1.5 \pm 0.5}$. Strong similarities in morphology and general physical conditions were found to exist among all of the southern clouds in the sample.

Subject Headings: Infrared: Sources - Stars: Formation - Nebulae: General

I. INTRODUCTION

High surface brightness 1.0 mm continuum emission has been detected from dust clouds associated with the seven southern HII regions RCW 38, RCW 57, G333.6-0.2, RCW 117, RCW 122, G351.6-1.3 and W33/W33A. All of the sources are located in the inner part of the Galaxy near the galactic plane. They were selected from among the brightest southern hemisphere 10 μ sources observed by Frogel and Persson (1974) and Frogel et al. (1977), with the aim of determining the distribution of dust in the vicinity of compact HII regions associated with dense molecular clouds.

An additional source, NGC 6334, has previously been discussed in detail by Cheung et al. (1978). As part of our 1.0 mm continuum survey, we also observed several extragalactic objects, including mapping of the 30-Doradus region in the Large Magellanic Cloud, the results of which will be presented separately.

Five of the seven sources disucssed here were mapped extensively with one arc minute resolution. In each case, there is a close association between the 1.0 mm source, several compact near infrared objects, extended high surface brightness far infrared emission, and CO and OH/H_2O line emission (where observations are available). The 1.0 mm continuum maps have been used to determine the radial dust density distribution in the cores of these dense southern clouds for comparison with density distribution results for northern objects (Westbrook et al. 1976).

II. OBSERVATIONS

The observations were made during 1977 and 1978 with the 4-meter telescope at the Cerro Tololo Inter-American Observatory in Chile. Figure 1 shows a schematic of the remote controlled, prime focus infrared photometer (Gezari 1979) and the liquid helium cooled detector system. The oscillating tertiary mirror, onto which the primary is imaged, and reactionless drive assembly are dynamically balanced to minimize synchronously-induced detector microphonic noise. The motion of the wobbling mirror is generated by a servo-controlled magnet driver system capable of producing an 80% efficient square wave cycle at 15 Hz with a stable beam separation of up to 8 arc min on the sky. The amplitude and position angle of the beam separation are variable and were typically set at 5 arc min in right ascension at a switching frequency of 10 Hz.

The detector in 1977 was a composite bolometer (Hauser and Notarys 1975) consisting of a Germanium thermometer mounted on a 2 mm square bismuth-coated sapphire substrate, with an electrical NEP of 1×10^{-14} W $Hz^{-\frac{1}{2}}$ at $1.4^{o}K$. For the 1978 observations, a bismuth-coated diamond substrate composite bolometer with an electrical NEP of 8×10^{-15} W $Hz^{-\frac{1}{2}}$ was used. The output of the bolometer was DC-coupled to a cooled buffer amplifier inside the liquid helium dewar. A parabolic light cone (Harper et al. 1976) acting as a field lens in the focal plane concentrated the beam on to the detector in an integrating cavity. Background radiation of wavelength less than 600 μm was rejected by an 8-layer capacitive mesh

low pass filter and a fluorogold filter at liquid helium temperature, and by a black polyethylene window on the 77°K radiation shield. The overall observational spectral band was further limited by the atmospheric transmission to wavelengths longer than 800 μm and by diffraction effects to wavelengths shorter than 1.5 mm. The size of the beam was adjustable with a cold aperture at the focal plane and was set at the diffraction limited beamwidth of 65 arc sec (FWHP) during most of the observations.

The positional accuracy of the observations was limited by the setting accuracy of the 4-m telescope. Absolute positional calibration was achieved by systematic measurement of visible stars and submillimeter flux calibrators to develop an error map for alignment of the telescope mount and telescope flexure, and to compensate for differential atmospheric refraction. Therefore the positions observed are accurate to within 10 arc sec.

Measurements were generally made in a grid with spacings of 1 arc min. Data points separated by one beam separation were deconvolved to correct for the effects of beam switching on an extended source. A combined atmospheric transmission-extinction curve was made by frequent measurements of a bright reference point within the sources being observed. The signal at each map grid point was subsequently corrected and normalized relative to the reference point. The normalized signals taken on different days were averaged together. The 1 σ statistical error associated with each normalized data point was typically less than 5% of the peak flux density.

Flux calibration of the maps was made using Saturn, Venus, and Sgr B2 as the photometric standards. The flux-weighted mean wavelength and flux

density were calculated using the atmospheric modelling procedure discussed by Elias et al. (1978). We adopted 1.0 mm brightness temperatures of 145 ± 7°K for Saturn, 276 ± 14°K for Venus (Werner et al. 1978), and a flux density of 390 Jy ± 80 Jy into a 65 arc sec beam for Sgr B2 (Cheung et al. 1978). The calibrated fluxes obtained on different days and from using different photometric standards were compared and averaged together, with a statistical deviation from the mean of less than 15% in most cases. The total uncertainty in the absolute flux level was about 20%, mainly due to calibration uncertainties. The observational sensitivity of the system was limited to about 70 Jy $Hz^{-1/2}$ by small scale atmospheric opacity variations between the two chopped beams. However, during the usable portions of the four observing sessions, atmospheric transmission variations were judged to be too small to produce a significant deviation from the effective wavelength of 1.0 ± 0.1 mm.

III. RESULTS AND ANALYSIS

a) Nature of the 1.0 mm emission:

Figures 2-3 present 1.0 mm continuum maps for five of the 1.0 mm sources observed. The sources RCW 117 and G351.6-1.3 were not mapped extensively, so only their peak flux densities are presented (Table I). The most obvious characteristic of the mapped regions is that, in each case, the 1.0 mm emission has a central peak which is generally coincident with one or more of the compact sources in the 1 μ to 25 μ region observed by Frogel and Persson (1974) and Frogel et al. (1977). Furthermore, the broad 1.0 mm peaks are found at roughly the same positions as the intense 40-350 μm emission (Emerson et al. 1973, Furniss et al. 1975). Table I summarizes the observations at 1.0 mm and compares the positions and sizes of the 1.0 mm, radio, and near infrared sources. The observed ratio of the 40-350 μm flux to the 1.0 mm flux is generally consistent with the value expected for optically thin thermal emission from dust grains. A smooth extrapolation of the radio spectra (Figure 4) shows that, generally, not more than one third of the observed 1.0 mm flux in the cloud core may be attributed to the free-free process, assuming that the extent of the ionized region is comparable to, or smaller than, our beam size. Furthermore, in each case this process does not appear to contribute more than 10% of the total 1.0 mm flux observed from the entire extended region mapped.

The size of the optical and radio continuum HII regions listed in Table I is generally less than one arc minute. It is assumed that most of the ionized gas emission is confined to within the central 65 arc second beam area in each source (with the exception of the more extended source RCW 38). This assumption is supported by recent high resolution

observations of [Ne II] line emission in G333.6-0.2 (Aitken et al. 1977), and radio interferometric maps of W33 (Goss et al. 1978) and G351.6-1.3 (Broderick and Brown, 1974). The extrapolated 1.0 mm free-free flux density was subtracted from the peak 1.0 mm flux density in deriving dust emission properties for the sources discussed in the following sections.

b) Dust Optical Depth and Column Density:

The 1.0 mm continuum observations provide a direct probe of the distribution of matter in dense molecular clouds. In all known 1.0 mm sources, the 1.0 mm continuum dust emission is optically thin. The intensity of the 1.0 mm emission is proportional to the temperature and number density of the dust grains for dust temperature $T_d \gtrsim 25^{\circ}K$. The interpretation of the 1.0 mm continuum observational results is therefore relatively straightforward. In contrast, the gas density distribution inferred from ^{13}CO observations is accurate only under the assumptions of LTE (Dickman 1976), and constant abundance ratio of ^{13}CO to H_2, both of which may not hold uniformly throughout the molecular cloud.

The dust column density D projected along a line of sight through a dust cloud can be inferred from the observed 1.0 mm flux density S_ν using the relationship $D = (4/3)\rho_d \tau/(Q/a)$ (Westbrook et al. 1976) where ρ_d is the bulk density of the dust grains with radius a and 1.0 mm extinction efficiency factor Q. The optical depth τ is derived from the relation for optically thin emission $S_\nu \propto \tau B_\nu$, where B_ν is the Planck function at a grain temperature T_d. For grain temperature higher than $25^{\circ}K$, B_ν and hence D depend linearly on the dust temperature T_d. The largest uncertainty in the expression for D is the value of Q/a, which may vary

by more than an order of magnitude for different grain materials (Aannested 1975, Leung 1976). The derived parameters in Table II were calculated assuming the nominal values $T_d = 40^oK$ (see IIId), $\rho_d = 1$ gm cm^{-3}, $Q/a = 1\ cm^{-1}$ (Aannested 1975). Extensive molecular line observations are not available for the sources in Table II. For comparison with other molecular clouds, the predicted gas properties have been calculated by assuming a gas to dust mass ratio of 100 and a spherically symmetric source geometry.

c) Dust Temperature:

Useful estimates of the dust temperature and emissivity index may be obtained from a two parameter model fit to the ratio of the observed 40-350 μm and 1.0 mm fluxes for each source (Cheung et al. 1978), assuming that the 40-350 μm radiation and the excess 1.0 mm emission are both attributable to optically thin dust emission from the same extended dust cloud. Using an empirical emissivity law $\epsilon_\nu \propto \nu^n$ for individual dust grains, an average dust temperature was derived for the two cases n = 1 and 2. The results (Table II) are rather insensitive to errors in the observed flux ratio provided that the grain temperature is less than about 70^oK. The use of this derived average temperature for the region outside the central sub-arc-minute peak is reasonable since the dust temperature in a centrally heated molecular cloud is expected to fall off slowly with radial distance, $T(r) \propto r^{-0.4}$ (Scoville and Kwan 1976).

The above procedure applied to observations of OMC-1 by Westbrook et al. (1976) yielded an average temperature of $T = 60^{o}K$ for $n = 1$, which is close to the $70^{o}K$ in the central 1 arcmin and about $55^{o}K$ in the outlying region obtained for $n = 1$ from multicolor far infrared photometry (Werner et al. 1976). The dust temperature range quoted in Table II is generally higher than the observed ^{12}CO antenna temperature measured with a similar beam size (Gillespie et al. 1977), in qualitative agreement with observations of other molecular clouds and with the picture that the molecular gas is heated collisionally by dust grains.

d) Radial Density Distribution:

The projected 1.0 mm source surface brightness profile can be used as a basis for inferring the radial dust density distribution $\rho_d(r)$ of the cloud. As discussed in III(a), it has been assumed that the bulk of the free-free emission is not resolvable by the 65" beam and that the bulk of the gas emission is confined to within the central 1 arc min region. The dust emission profile may then be inferred by subtracting the extrapolated free-free flux density (Figure 4) from the peak of the observed 1.0 mm emission profile.

Figure 5 shows the model and observed 1.0 mm emission profiles projected along the line of sight for the five mapped sources. The averaged North-South and East-West dust emission intensity profiles of RCW 38, RCW 57, RCW 122, and W33 correspond to a radial dust density model distribution outside the central 1 arc min source core of $\rho_d(r) \propto r^{-1.5\pm.5}$. In this analysis it was assumed that the radial temperature distribution $T_d(r)$ decreases as $r^{-0.4}$ as predicted by the

radiative transfer model calculation of Scoville and Kwan (1976). If the ionized gas emission is more extended than 1 arc minute, the dust density profiles would have a steeper gradient than is illustrated in Figure 5. The observed density distribution in six northern 1.0 mm sources (Westbrook et al. 1976) also decreases rather steeply with radial distance, typically as $r^{-1.5}$ to r^{-2}.

IV. COMMENTS ON INDIVIDUAL SOURCES

a) RCW 38

Within the positional uncertainties, the 1.0 mm peak emission in RCW 38 is found at the same location as the 40-350 μm and ^{12}CO line emission peaks. Four compact infrared sources (Frogel and Persson 1974) and an H_2O maser source (Kaufmann et al. 1976) are located inside the 0.6 contour at 1.0 mm. The 1.0 mm source is similar in shape to the radio source, but is clearly more extended. The extrapolated radio spectrum of RCW 38 (Figure 4) is much steeper than the $\nu^{-0.1}$ dependence expected for an optically thick free-free thermal spectrum. However, the turnover at $\lambda > 10$ cm indicates it is not a non-thermal source.

The entire 1.0 mm source coincides with a strong CO emission peak inside a molecular complex extending about 30' x 30' in area (Gillespie et al. 1979). All of the radio, molecular, and infrared emission sources lie in a heavily obscured region close to an area of bright optical nebulosity.

b) RCW 57

The peak flux density at 1.0 mm is found about 30" to the west of a cluster of five 1-25 μm sources, including one BN-type object (Frogel and Persson 1974). The steep gradient to the west and extended source contours to the east at 1.0 mm follow a similar but narrower profile in the 10 μm map. An H_2O maser source is located within the 10 μm cluster, but no OH emission was observed (Caswell et al. 1977). This source was measured at 1 mm with a 2 arc min beam by Arnold et al. (1978), but their reported flux density is substantially less than the value obtained in this work. The half power source size of RCW 57 (corrected for beam size) is somewhat larger at 1.0 mm than at radio wavelengths. The 1.0 mm source generally coincides with an optical extension to the south of the optical RCW 57 nebula.

c) G333.6-0.2

G333.6-0.2 is the only southern HII region which has been observed with high spatial resolution (1' or less) across the infrared and submillimeter spectrum. The surface brightness peaks at 1.0 mm, 200 μm, 100 μm, 50 μm (Hyland et al. 1979), 12.8 μm (Aitken et al. 1977), and 2-20 μm (Becklin et al. 1973) all coincide to within positional uncertainties. Figure 6 is a plot of the observed source size (corrected for beam size) as a function of wavelength. The dramatic increase in source size between about 30 μ and 300 μ suggests the presence of a very cool, diffuse dust envelope surrounding the luminous far infrared source observed by Hyland et al. (1979). The 1.0 mm source also coincides with, and is considerably more extended than, the ionized gas emission region. Free-free emission probably contributes significantly to the observed 1.0 mm flux in the central 1 arc min core.

G333.6-0.2 shows a particularly flat brightness distribution near the source center. Observationally this circularly symmetric plateau structure may be interpreted either as a uniform dust column density distribution, or as a dust-depleted region at the center of a spherical source. The latter possibility was considered in a model calculation, in which the central 1 arc minute of the model cloud was depleted of dust. The observed profile of G333.6-0.2 is not inconsistent with the model for dust depletion. Dust depletion in the compact (20") ionized core of G333.6-0.2 has been suggested by Aitken et al. (1977) from a comparison of the projected line and continuum intensities at 12.8μm. However, the uniform column density case is also viable.

d) RCW 117 (H2-3)

This source has not been mapped completely at 1.0 mm. Most of the 1-25 μm flux was observed to originate from a single extended component about 110 arcsec in diameter (Becklin et al. 1974). RCW 117 is the weakest of the eight 1.0 mm sources observed, yet it is one of the more intense 40-350 μ sources, with $L_{IR} \sim 2 \times 10^6 L_\odot$ (Emerson and Jennings 1973).

e) RCW 122

Both the 1.0 mm and 10 μm emission (Frogel et al. 1977) in RCW 122 are extended roughly in the north-south direction. Two compact infrared sources and an H_2O maser source are located within the 0.6 contour of the 1.0 mm map. An OH maser source was also found toward the edge of the 1.0 mm map (Caswell et al. 1977). The entire 1.0 mm source is embedded inside a 25 x 30 arcmin CO molecular cloud (Gillespie et al. 1979), but the 1.0 mm emission peak is found to be located approximately 3 arcmin south of the main ^{12}CO peak. The 1.0 mm source is associated wi intense 40-350 μm emission, and the total infrared luminosity of RCW 122 is $3 \times 10^6 L_\odot$ at a distance of about 5 kpc. The 1.0 mm flux density reported by Arnold et al. (1978) is considerably less than the value reported here.

f) G351.6-1.3

G351.6-1.3 has not been mapped completely at 1.0 mm. A flux density of 42 Jy at 1.0 mm was measured with a 65 arc sec beam at the position of the compact 10 μm source. This value is consistent with the flux density of 67 Jy into a 2 arcmin beam reported by Arnold et al. (1978).

g) W33 and W33A

The main 1.0 mm peak emission in W33 coincides with a cluster of compact near infrared sources (Dyck et al. 1977) associated with the compact HII region G12.8-1.0. A second unresolved 1.0 mm peak is found at the same position as the OH emission line object W33A, and a compact 2-20 μm object similar to the BN source in Orion (Capps et al. 1978). The high resolution radio interferometric map of Goss et al. (1978) shows that the size of the HII continuum source W33 is less than 40" at 2.8 cm, considerably less than the size of the 1.0 mm source. No significant radio continuum emission has been observed at W33A or in the region between the two 1.0 mm sources. The ratio of 1.0 mm flux density between W33A and W33 is about 0.3, while the 2.8 cm flux density ratio is less than 4×10^{-3}, suggesting that W33A is a much younger dust condensation in the evolutionary sequence leading to the formation of a luminous HII region.

V. CONCLUSION

The southern hemisphere 1.0 mm sources presented here were found to have a narrow range of dust column density (6 to 30 x 10^{-3} gm cm^{-2}), linear extent (1.5 to 3 pc), total mass (2 to 10 x 10^4 $M_\odot$) and infrared luminosity (2 to 4 x 10^6 $L_\odot$). In all cases the dense, extended dust envelopes are singly peaked and centered about one or more compact near infrared sources.

A fairly steep gradient in the dust distribution around the central peaks is found in most of the sources, consistent with a radial density distribution function $\rho(r) \sim r^{-1.5 \pm .5}$. This is in close agreement with the density profiles of other extended 1.0 mm continuum sources differing from our sample in mass, linear extent, and infrared luminosity: OMC-1, Sgr B2, W3, W49, DR 21, and W75 (Westbrook et al. 1976). The similarity in radial density distributions in view of the large range of masses and sizes provides further evidence that the extended dense clouds surrounding compact energetic sources form by a rather general physical process.

All of the sources selected for observation on the basis of their 10 μ emission were found to be strong, extended 1.0 mm sources, establishing a strong correlation between the two source types. The present lack of ample high spatial resolution observations at far infrared, CO, and radio continuum wavelengths precluded a detailed comparison with the 1.0 mm maps presented here. However, in each case where observations at other wavelengths are available, there was found to be a close association between the 1.0 mm source and the extended far infrared emission, carbon

monoxide and OH/H_2O maser emission. Two notable exceptions are the 1.0 mm source W33A, which is not associated with any significant ionized gas emission, and the 1.0 mm source RCW 122, which is displaced by 3 arc minutes from the main ^{12}CO peak. These two sources are thus similar in some respects to the 1.0 mm sources NGC 6334 I and II previously discussed by Cheung et al. (1978). It is likely that the same dust material gives rise to both the 1.0 mm and far infrared emission from the sources listed in Table I, and that their luminosity is provided principally by heavily obscured young stars or stellar associations embedded within the dust clouds.

ACKNOWLEDGMENTS

We are grateful to Dr. V. Blanco, Director of Cerro Tololo Inter-American Observatory, and the technical staff for the support and cooperation they have given to the 1.0 mm observing program. We also thank Dr. M. W. Werner for supplying us with data prior to publication, Dr. M. Simon for helpful discussions, Dr. P. Goldsmith for valuable comments regarding molecular gas abundance ratios, Dr. R. H. Hildebrand and his colleagues for fabricating light cone optics, and Dr. K. Moeller for fabricating infrared filters for our instrument. This work is funded by the National Aeronautics and Space Administration and the National Science Foundation.

REFERENCES

Aannestad, P. A., 1975, Ap. J., 200, 30.

Aitken, D. K., Griffiths, J., and Jones, B., 1977, M.N.R.A.S., 179, 179.

Arnold, E. M., Kreysa, E., Schultz, G. V., and Sherwood, W. A., 1978, Astron. Astrophys., 70, L1.

Balick, B., 1972, Ap. J., 176, 353.

Becklin, E. E., Frogel, J. A., Neugebauer, G., Persson, S. E., and Wynn-Williams, C. G., 1973, Ap. J., 182, L 125.

Becklin, E. E., Frogel, J. A., Kleinmann, D. E., Neugebauer, G., Persson, S. E., Wynn-Williams, C. G., 1974, Ap. J., 187, 487.

Broderick, J. J., and Brown, R. L., 1974, Ap. J., 192, 343.

Brown, R. L., and Broderick, J. J., 1973, Ap. J., 181, 125.

Capps, R. W., Gillett, F. C., and Knacke, R. F., 1978, Ap. J., 226, 863.

Caswell, J. L., and Robinson, B. J., 1974a, Aust. J. Phys., 27, 495.

Caswell, J. L., and Robinson, B. J., 1974b, Aust. J. Phys., 27, 597.

Caswell, J. L., Haynes, R. F., and Goss, W. M., 1977, M.N.R.A.S., 181, 427.

Cheung, L., Frogel, J. A., Gezari, D. Y., and Hauser, M. G., 1978, Ap. J., 226, L 149.

Dickman, R. L., 1976, Ph. D. Thesis, Columbia Univ.

Dyck, H. M., and Simon, T., 1977, Ap. J., 211, 421.

Elias, J. H., Ennis, D. J., Gezari, D. Y., Hauser, M. G., Houck, J. R., Lo, K. Y., Matthews, K., Nadeau, D., Neugebauer, G., Werner, M. W., and Westbrook, W. E., 1978, Ap. J., 220, 25.

Emerson, J. P., Jennings, R. E., and Moorwood, A. F. M., 1973, Ap. J., 184, 401.

Emerson, J. P., and Jennings, R. E., 1978, Astron. & Astrophys., 69, 129.

Frogel, J. A., and Persson, S. E., 1974, Ap. J., 192, 351.

Frogel, J. A., Persson, S. E., and Aaronson, M. 1977, Ap. J., 213, 723.

Furniss, I., Jennings, R. E., and Moorwood, A. F. M., 1975, Ap. J., 202, 400.

Gardner, F. F., Robinson, B. J., and Sinclair, M. W., 1976, Aust. J. Phys., 29, 211.

Genzel, R., and Downs, D., 1977, Astr. & Ap. (Supp.), 30, 145.

Gezari, D. Y., 1979, (preprint).

Gillespie, A. R., Huggins, P. J., Sollner, T. C. L. G., Phillips, T. G., Gardner, F. F., and Knowles, S. H., 1977, Astr. & Ap., 60, 221.

Gillespie, A. R., White, G. J., and Watt, G. D., 1979, M.N.R.A.S., 186, 38.

Goss, W. M., and Shaver, P. A., 1970, Aust. J. Phys. (Suppl.), 14, 1.

Goss, W. M., Matthews, H. E., and Winnberg, A., 1978, Astr. & Ap., 65, 307.

Goss, W. M., Radhakrishnan, V., Brooks, J. W., and Murray, J. D., 1972, Ap. J. (Suppl.), 24, 123.

Harper, D. A., Hildebrand, R. H., Stiening, R., and Winston, R., 1976, Applied Optics, 15, 53.

Hauser, M. G., and Notarys, H., 1975, B.A.A.S., 7, 409.

Hyland, A. R., Ellis, M. J., Robinson, G., Thomas, J. A., Becklin, E. E., Gatley, I., and Werner, M. W., 1979, in preparation.

Johnston, K. L., Robinson, B. J., Caswell, J. L., and Batchelor, R. A., 1972, Ap. L., 10, 93.

Kaufmann, P., Gammon, R. H., Ibanex, A. C., Lepine, J. R. D., Marques Dos Santos, P., Paes de Burros, M. H., Scalise, E., Schaal, P. E., Zisk, S. H., Carter, J. C., Meeks, M. L., and Sobolewski, J. M., 1976, Nature, 260, 306.

Knowles, S. H., Batchelor, R. A., 1978, M.N.R.A.S., 184, 107.

Leung, C. M., 1976, Ap. J., 199, 340.

McGee, R. X., Lynette, M. Newton, and Batchelor, R. A., 1975, Aust. J. Phys., 28, 185.

Radhakrishnan, V., Goss, W. M., Murray, J. D., and Brooks, J. W., 1972, Ap. J. Suppl., 24, 49.

Scoville, N. Z., and Kwan, J., 1976, Ap. J., 206, 718.

Shaver, P. A., and Goss, W. M., 1970, Aust. J. Phys. (Suppl.), 14, 133.

Werner, M. W., Gatley, I., Harper, D. A., Becklin, E. E., Loewenstein, R. F., Telesco, C. M., and Thronson, H. A., 1976, Ap. J., 204, 420.

Werner, M. W., Neugebauer, G., Houck, J. R., and Hauser, M. G., 1978, preprint.

Westbrook, W. E., Werner, M. W., Elias, J. H., Gezari, D. Y., Hauser, M. G., Lo, K. Y., and Neugebauer, G., 1976, Ap. J., 209, 94.

Wright, E. L., 1973, Ap. J., 185, 569.

ADDRESSES OF THE AUTHORS:

L. H. Cheung, D. Y. Gezari, and M. G. Hauser

Laboratory for Extraterrestrial Physics, Code 693.2

NASA Goddard Space Flight Center

Greenbelt, Maryland 20771

J. A. Frogel

Cerro Tololo Inter-American Observatory

Casilla 63-D, La Serena

Chile

TABLE 1. OBSERVATIONAL SOURCE PROPERTIES

Source	Emission Peak Positions*						1.0 mm Flux Density†			Source Size (FWHM)‡			Associated§ Emission
	1.0 mm Continuum		10 μm		Radio		Central 65" (Jy)	Total (Jy)	Extrapolated free free (Jy)	1.0 mm (arcmin)	10 μm (arcsec)	Radio (arcmin)	
	α(1950)	δ(1950)	Δα	Δδ	Δα	Δδ							
RCW 38	$08^h57^m20^s.9$	$-47^\circ18'50''$	$+3^s.3$	0"	$+2^s.5$	-28"	128	1.5×10^3	40	3 x 2	9	1.3x2.0	CO, H_2O
RCW 57	$11^h09^m43^s.9$	$-61^\circ02'09''$	$-0^s.6$	0"	$+2^s.1$	-27"	146	1.3×10^3	55	2	22.5	0.9	H_2O
G333.6-0.2	$16^h18^m23^s.0$	$-49^\circ58'54''$	$+0^s.5$	-4"	$+3^s$	+ 0"	139	6.8×10^2	50	2	9	0.9x0.8	CO, H_2O
RCW 117	$17^h06^m01^s.5$	$-41^\circ32'20''$	0^s	0"	$+6^s.5$	+26"	31	-	-	-	49	1.7	CO
RCW 122	$17^h16^m40^s.1$	$-38^\circ54'18''$	$+0^s.5$	0"	$-1^s.1$	-18"	53	3.4×10^2	16	1 x 2	24	1	CO, H_2O, OH
G351.6-1.3	$17^h25^m53^s.0$	$-36^\circ37'49''$	0^s	0"	$+3^s$	-19"	42	-	6	-	-	0.1	
W 33	$18^h11^m18^s.1$	$-17^\circ56'28''$	$+0^s.2$	-2"	$+0^s.4$	- 5"	132	5.5×10^2	28	2	5x20	< 0.8	H_2O
W 33A	$18^h11^m43^s.7$	$-17^\circ53'02''$	-	-	$+0^s.6$	- 9"	41	98	0.7	1	-	-	OH

* Offsets from the 1.0 mm peak positions observed here to the 10 μm and radio peaks are given by Δα in right ascension and Δδ in declination. The 10 μm positions are taken from measurements by Frogel and Persson (1974), Frogel et al. (1977). The radio positions are from 5 GHz measurements by Goss and Shaver (1970). The positional uncertainties are ±10" for the 1-mm peaks, ±4" for the 10 μm peaks, ±1' for the radio peaks. The radio positions for W 33 and W 33A are taken from Goss et al. (1978) with a quoted positional error of ±5".

† Peak flux densities in our 65 arcsec (FWHP) beam and total flux density within the 0.1 contour have calibration uncertainties of about 20%. The extrapolated free-free flux density contribution an 1.0 mm is obtained from Figure 4.

‡ 10 μm size from Frogel and Persson (1974), Frogel et al. (1977) and Dyck and Simon (1977), radio size from Shaver and Goss (1970) except for G351.6-1.3 (Broderick and Brown 1974) and W33 (Goss et al. 1978).

§ All sources have associated 40-350 μ emission observed by Emerson et al. (1973) and Furness et al. (1975); CO observations by Gillespie et al. (1977, 1979); OH and H_2O emission line/maser sources from Kaufmann et al. (1976), Knowles and Batchelor (1977), Caswell et al. (1977) and Genzel and Downs (1977).

TABLE 2. CALCULATED PARAMETERS

Source	Distance* (kpc)	Flux Ratio† 40-350μm/1.0 mm	Average Dust‡ Temperature (K) $\varepsilon_\nu \propto \nu^1$	Average Dust‡ Temperature (K) $\varepsilon_\nu \propto \nu^2$	^{12}CO T_A§ (K)	D_{dust} (gm cm^{-2})	N_{H_2} (cm^{-2})	n_{H_2} (cm^{-3})	A_V (mag)	Total M_{gas} ($M_\odot$)	L_{IR} ($L_\odot$)
RCW 38	1.5	4.3×10^3	40	22	11.3	2.6×10^{-2}	8.0×10^{23}	6.1×10^5	800	3×10^4	4×10^5
RCW 57	3.6	-	-	-	29	2.4×10^{-2}	7.6×10^{23}	2.4×10^5	700	9×10^4	-
G 333.6-0.2	4.5	7.6×10^3	47	25	14.2	1.8×10^{-2}	5.5×10^{23}	1.4×10^5	500	1×10^5	4×10^6
RCW 117	4	-	-	-	10.9	6.4×10^{-3}	1.9×10^{23}	5.3×10^4	200	-	2×10^6
RCW 122	5	7.0×10^3	44	24	33	7.9×10^{-3}	2.4×10^{23}	5.4×10^4	200	5×10^4	3×10^6
G 351.6-1.3	-	-	-	-	-	8.0×10^{-3}	2.3×10^{23}	-	200	-	2×10^6
W 33	4.6	-	-	-	-	2.2×10^{-2}	6.6×10^{23}	1.7×10^5	700	7×10^4	$>3\times10^6$
W 33A	4.6	-	-	-	-	8.5×10^{-3}	2.5×10^{23}	6.3×10^4	300	2×10^4	-

* Distances from Radhakrishnan et al. (1972), Goss et al. (1972).

† 40-350μ data from Emerson et al. (1973), Furniss et al. (1975). The flux ratio is calculated for the area within a 4' beam.

‡ Average dust temperature for the entire source determined from the model calculation of Cheung et al. (1978) for dust emissivities ε_ν.

§ CO data for comparison from Gillespie et al. (1977) measured with a 4.5 arcmin beam.

N.B. The derived parameters D_{dust}, N_{H_2}, n_{H_2} and A_V are measured along a line of sight thru the peak. Total M_{gas} refers to the derived gas mass within the 0.1 contour (see Figures 1 and 2), L_{IR} is the sum of the 1-25μ and 40-350μm luminosity.

ORIGINAL PAGE IS
OF POOR QUALITY

FIGURE CAPTIONS

Figure 1: Cross-sectional view of the remote controlled prime focus infrared photometer (Gezari 1979) used on the Cerro Tololo Inter-American Observatory 4-m telescope. A camera mirror re-images the 4-m primary at the wobbling tertiary mirror. A reactionless drive mechanism, operated by a servo-amplifier, produces an essentially vibrationless, 80% efficient square wave beam switching motion of the tertiary mirror at 15 Hz, with a beam separation variable up to 8 arcmin.

Figure 2: a) 1.0 mm continuum map of G333.6-0.2. The peak flux density of 139 Jy into a 65 arcsec (FWHP) beam was observed at the same position of the unresolved near infrared sources (Becklin *et al.* 1973), the H_2O maser (Knowles *et al.* 1978), and the compact HII region (Shaver and Goss 1970). The statistical error in each contour is typically less than 5% of the peak. The uncertainty in absolute flux calibration is about 20%.

b) 1.0 mm continuum map of RCW 38. The contours are normalized relative to the peak flux density of 128 Jy into a 65" beam. The crosses represent the compact near infrared sources from the observations of Frogel and Persson (1974). The square box marks the quoted position of the H_2O maser (Kaufmann *et al.* 1976). The dotted contours indicate an incomplete data set.

c) 1.0 mm continuum map of RCW 57. The peak flux density is 146 Jy into a 65" beam. The near infrared peaks are marked by the crosses and the solid square indicates the quoted position of an H_2O maser (Knowles and Batchelor 1978).

d) 1.0 mm continuum map of RCW 122. The contours are normalized to the peak flux density of 53 Jy into a 65" beam. The square box marks the H_2O maser (Caswell et al. 1977) and the crosses mark the two unresolved 10 μm sources.

Figure 3: 1.0 mm continuum map of the W33 and W33A region. The peak flux density is 132 Jy for W33 and 41 Jy for W33A into a 65 arcsec beam. Between the two 1.0 mm peaks, the observed 1.0 mm flux density is less than 10% of the maximum at W33. The square marks the position of the OH emission line source (Goss et al. 1978). No radio frequency HII emission has been detected near the 1.0 mm source at W33A, suggesting that it is a relatively young object.

Figure 4. Radio continuum spectra of five HII regions. The free-free flux density at 1.0 mm is estimated by extrapolation from the radio frequency data. The square data points represent the measured peak 1.0 mm continuum flux density into a 65 arcsec (FWHP) beam. Free-free emission may contribute as much as 30% to the observed 1.0 mm flux density in the central 1 arcmin of each object, but since the ionized regions are not much larger than 1' (Table I), the overall free-free contribution is typically less than 10% of the 1.0 mm flux density integrated over each map. The observational references are 408 MHz: Goss and Shaver (1970), 1.67 GHz: Caswell and Robinson (1974 b), 2.7 GHz: Caswell and Robinson (1974 a), 3.3 GHz: Gardner et al. (1976), 5 GHz: Shaver and Goss (1970), 8.9 GHz: McGee et al. (1975), 22 GHz: Johnston et al. (1972), 85 GHz: Brown and Broderick (1973), 1.0 mm: this work.

Figure 5: Spatial intensity profiles in right ascension (EW for east-west) and declination (NS for north-south) for five HII regions, from the 1.0 mm continuum maps (Figures 1 and 2). The model (dashed lines) shows the expected intensities at 1 arcmin intervals, in a 65 arcsec (FWHP) beam, from an optically thin, spherically symmetric dust cloud for the two cases of radial density distribution $\rho(r) \propto r^{-1}$ and r^{-2}. The extrapolated 1.0 mm free-free contribution in the central 65 arcsec (see Table I) has been subtracted from the profile of each source, and the scans normalized for comparison with the model.

The averaged NS and EW profiles of the HII regions RCW 38, RCW 57, RCW 122, and W33 are consistent with a radial density distribution $\rho(r) \propto r^{-1.5 \pm .5}$. The peculiar nature of the G333.6-0.2 profile may be attributable to central dust depletion, as discussed in the text.

Figure 6: The observed diameter of G333.6-0.2 (FWHM, corrected for beam size) plotted vs. wavelength. The data references are: 2.2μm and 10μm, Becklin et al. (1973); 30μm, 50μm, and 200μm, Hyland et al. (1979); 1.0μm, this work.

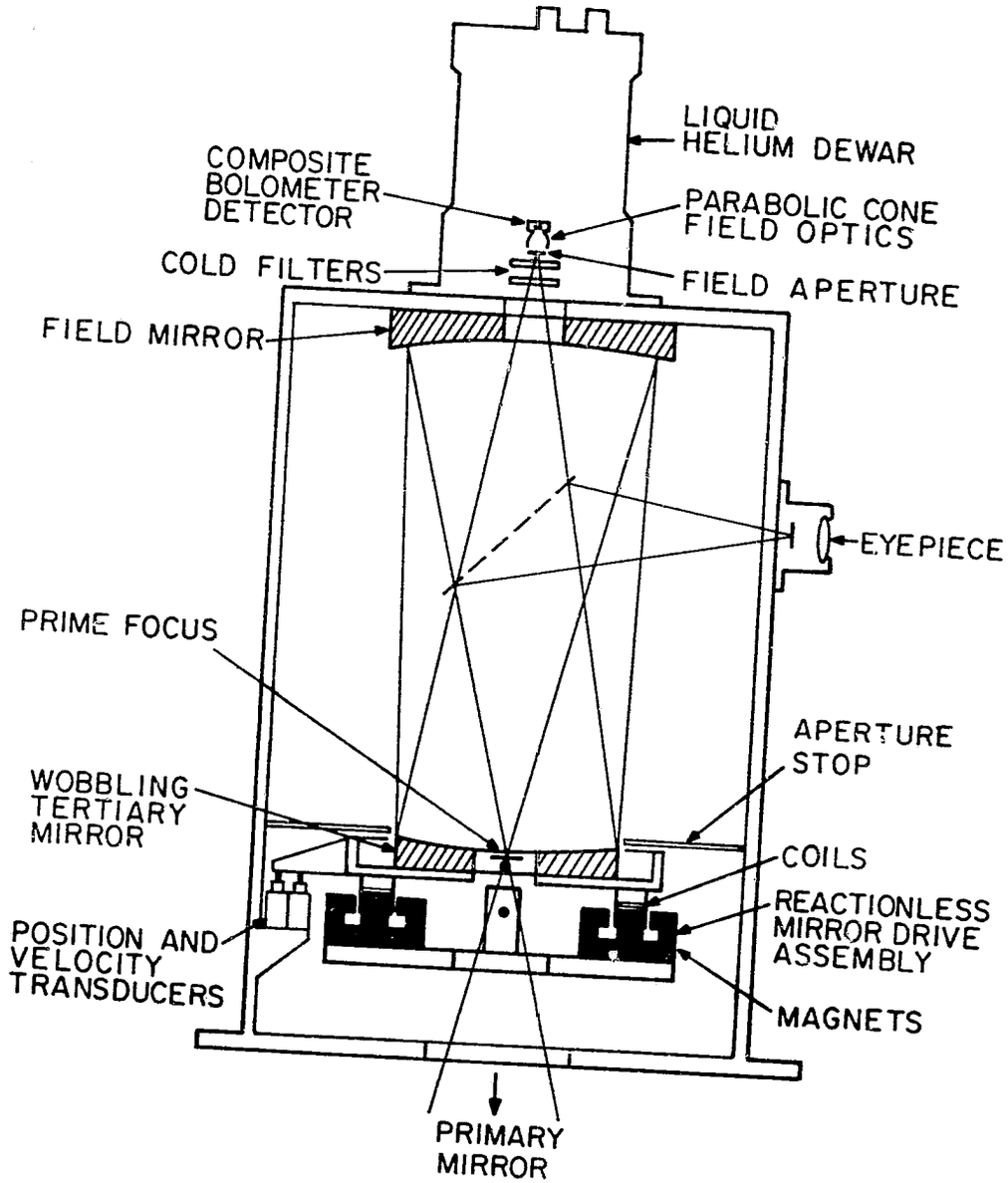

PRIME FOCUS PHOTOMETER

Figure 1

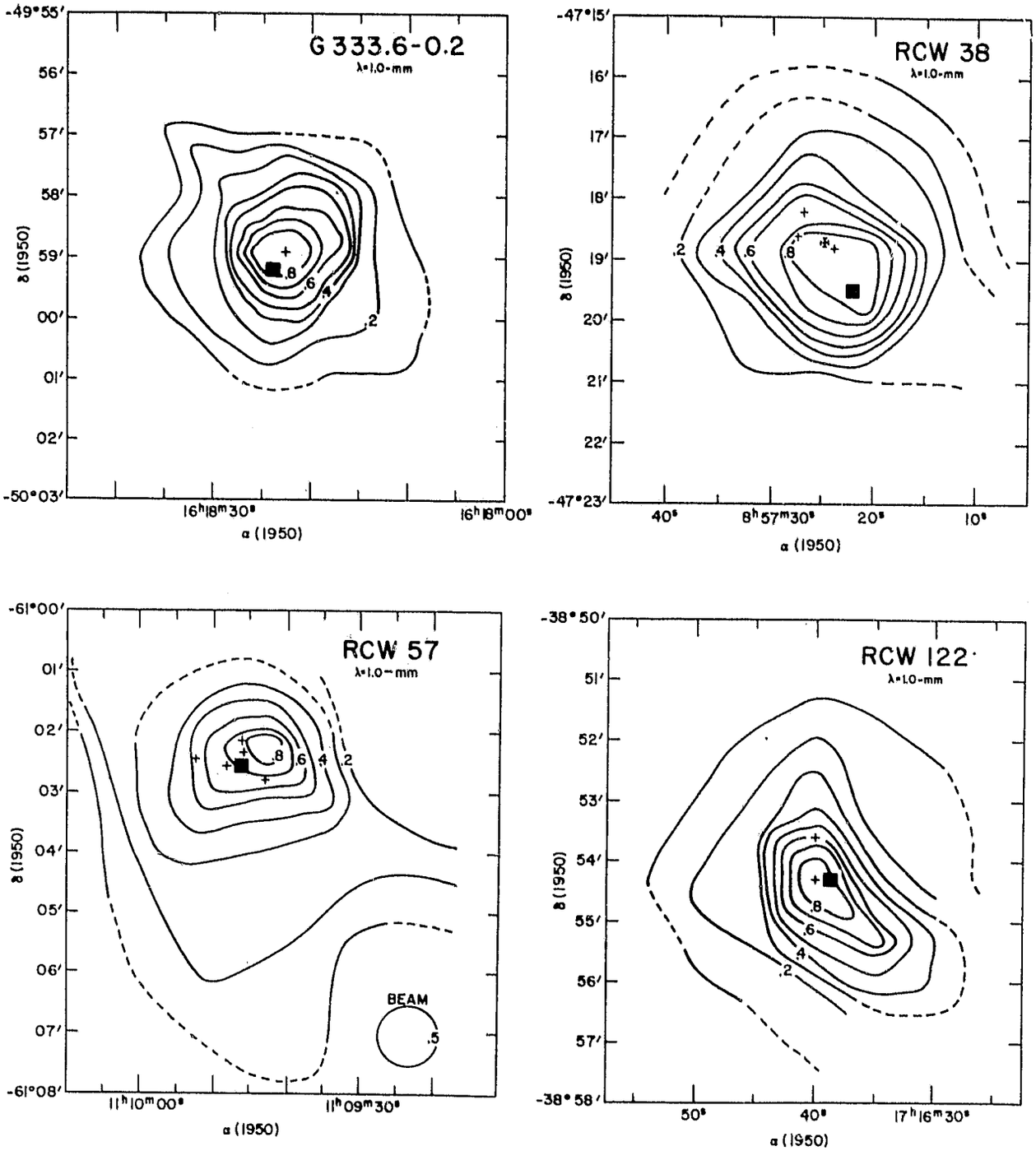
G 333.6-0.2
λ=1.0-mm
-49°55′
56′
57′
58′
59′
00′
01′
02′
-50°03′
δ (1950)
16h18m30s
16h18m00s
α (1950)
.8
.6
.4
.2
RCW 38
λ=1.0-mm
-47°15′
16′
17′
18′
19′
20′
21′
22′
-47°23′
δ (1950)
40s
8h57m30s
20s
10s
α (1950)
.2
.4
.6
.8
RCW 57
λ=1.0-mm
-61°00′
01′
02′
03′
04′
05′
06′
07′
-61°08′
δ (1950)
11h10m00s
11h09m30s
α (1950)
.8
.6
.4
.2
BEAM
.5
RCW 122
λ=1.0-mm
-38°50′
51′
52′
53′
54′
55′
56′
57′
-38°58′
δ (1950)
50s
40s
17h16m30s
α (1950)
.8
.6
.4
.2

Figure 2

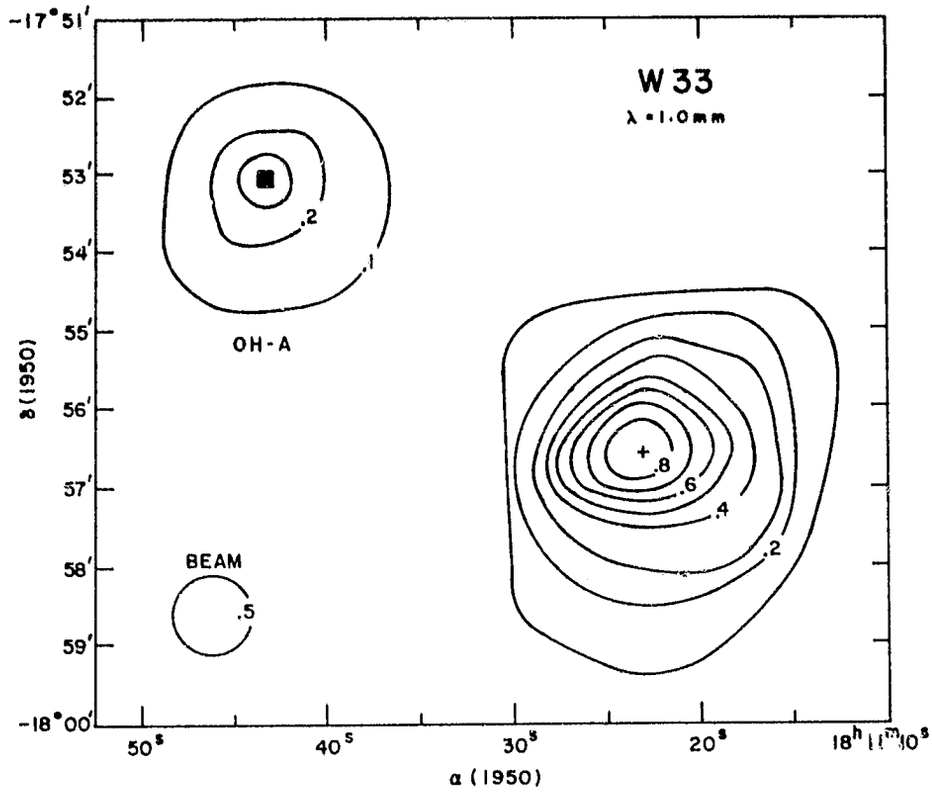
W 33
λ = 1.0 mm
OH-A
BEAM
.1
.2
.5
.8
.6
.4
.2
-17°51′
52′
53′
54′
55′
56′
57′
58′
59′
-18°00′
δ (1950)
50s
40s
30s
20s
18h 11m 10s
α (1950)

Figure 3

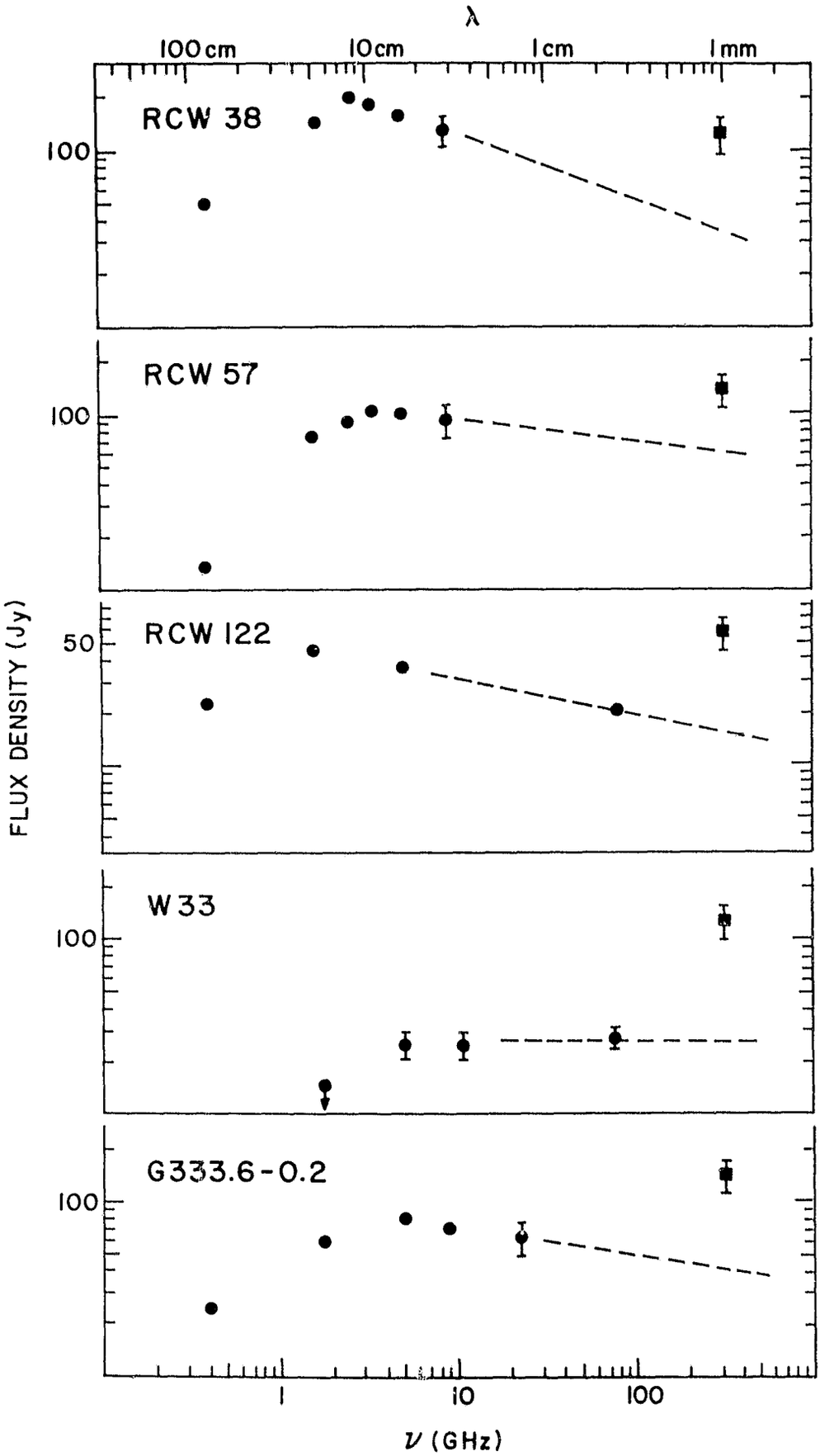
λ
100 cm
10 cm
1 cm
1 mm
RCW 38
RCW 57
RCW 122
W 33
G333.6-0.2
100
100
50
100
100
FLUX DENSITY (Jy)
1
10
100
ν (GHz)

Figure 4

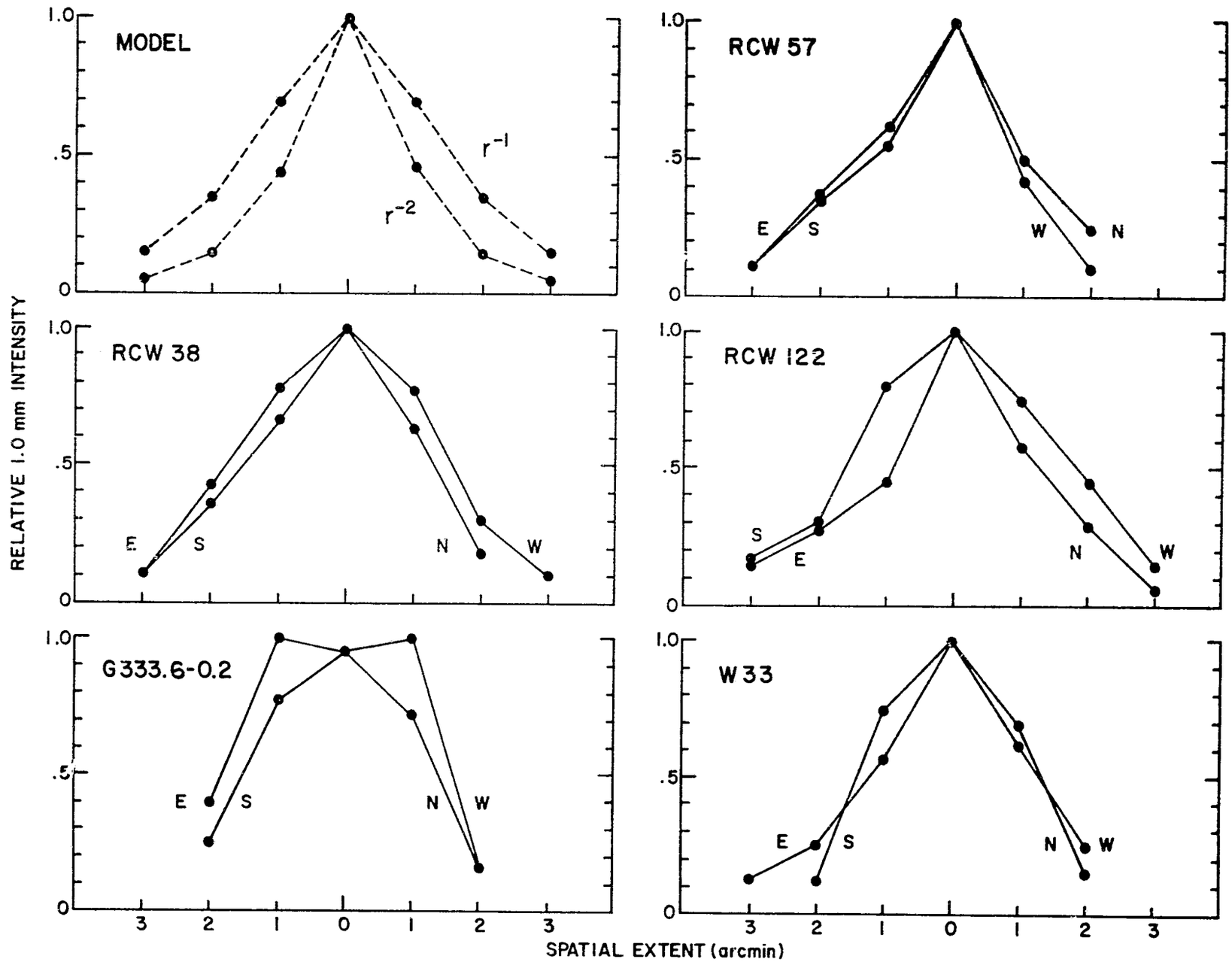
MODEL
r^{-1}
r^{-2}
RCW 57
E
S
W
N
RCW 38
E
S
N
W
RCW 122
S
E
N
W
G333.6-0.2
E
S
N
W
W33
E
S
N
W
1.0
.5
0
3
2
1
0
1
2
3
RELATIVE 1.0 mm INTENSITY
SPATIAL EXTENT (arcmin)

Figure 5

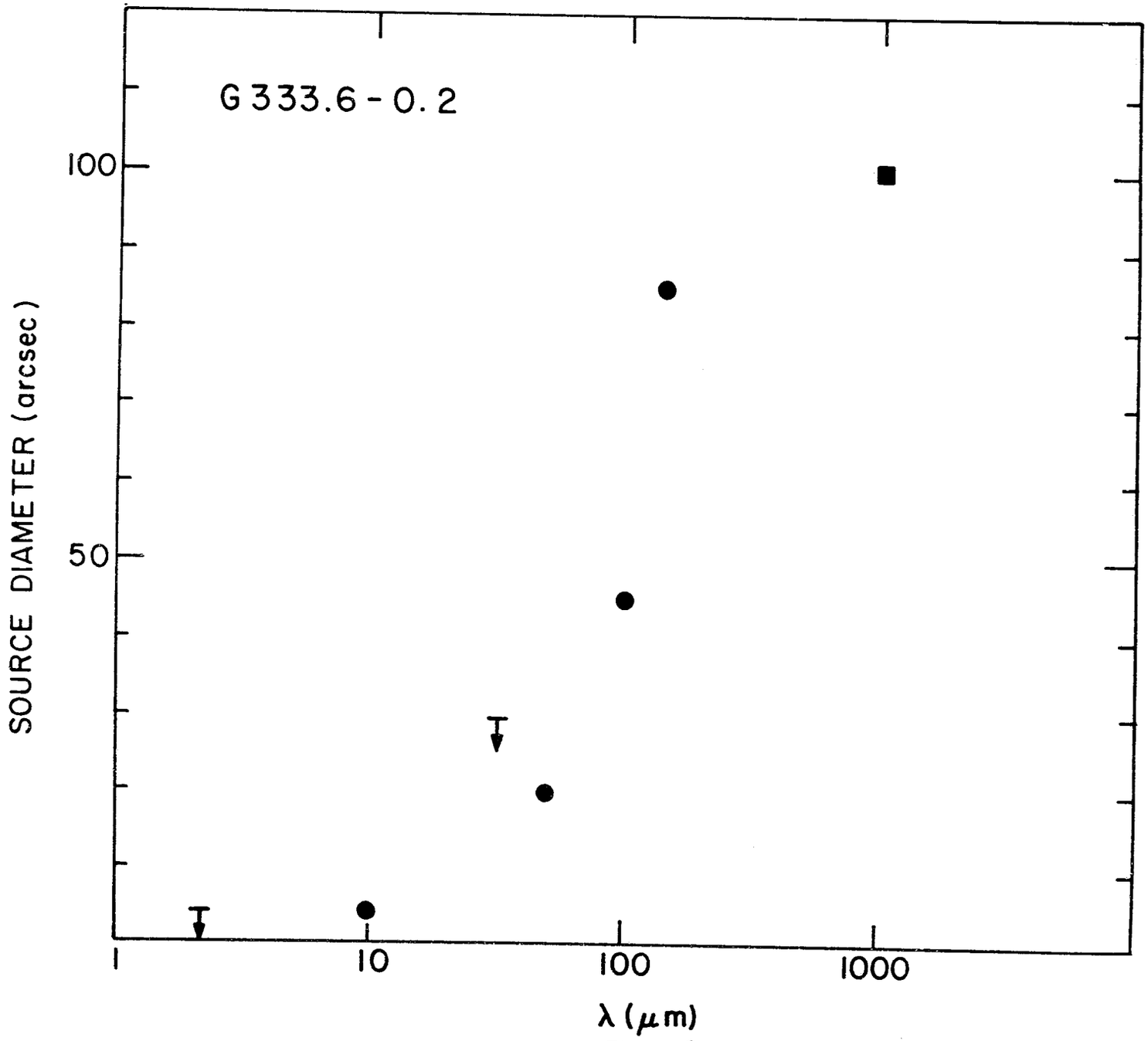

Figure 6